

# Fractal fronts in fractal fractures: large and small-scale structure

G. Drazner and J. Koplik

Benjamin Levich Institute and Department of Physics,  
City College of the City University of New York, New York, NY 10031

H. Auradou and J.P. Hulin

Laboratoire Fluide, Automatique et Systèmes Thermiques,  
UMR No. 7608, CNRS, Université Paris 6 and 11,  
Bâtiment 502, Université Paris Sud, 91405 Orsay Cedex, France.

(Dated: January 20, 2022)

## Abstract

The evolution and spatial structure of displacement fronts in fractures with self-affine rough walls are studied by numerical simulations. The fractures are open and the two faces are identical but shifted along their mean plane, either parallel or perpendicular to the flow. An initially flat front advected by the flow is progressively distorted into a self-affine front with Hurst exponent equal to that of the fracture walls. The lower cutoff of the self-affine regime depends on the aperture and lateral shift, while the upper cutoff grows linearly with the width of the front.

PACS numbers: 47.55.Mh, 05.40.-a, 92.40.Kf, 47.53.+n

Fractures are ubiquitous in the Earth's upper crust and in many materials of engineering interest, and their size varies over a broad range of length scales, from several meters in the case of faults down to the sub-micron scale of micro-cracks. The geometry of the fracture obviously influences any transport process within it, and in particular the hydraulic properties of rock fractures, crucial in such applications as hydrocarbon recovery, subsurface hydrology, and earthquake prediction. In these situations, transport generally involves flow through entire networks of fractures, and often through a porous matrix as well, but frequently the flow is dominated by channeling through particular fractures [1, 2], and therefore there is considerable interest in fully understanding flow through an individual fracture.

A key feature characterizing the pore space geometry of fractured materials is the experimental observation that the roughness of fracture surfaces is statistically described as a self-affine fractal structure over an appreciable range of length scales [3, 4]. This observation holds for both man-made [5, 6, 7] and natural fractures [8, 9], and for a broad variety of materials and length scales. We consider rock fracture surfaces without overhangs, whose height can be described through a single valued function  $z(x; y)$ , where  $(x; y)$  are Cartesian coordinates in the mean plane of the surface. Self-affinity means that the surface remains statistically invariant under the scale transformation  $z(x; y) = \lambda^H z(x/\lambda; y/\lambda)$ , where the Hurst exponent  $H$  characterizes the roughness of the surface, in that the fluctuation of the surface heights over a length  $L$  is given by  $\sigma_z(L) = \lambda^H (L=\lambda)$ . Here  $\lambda$  is the topography, defined as the horizontal distance over which fluctuations in height have a rms slope of one [9]. Experimental values of  $H$  are found to be close to 0.8, for most of the materials considered and independent of the fracture mode [5, 6, 7, 8, 9], with the exception of materials displaying intergranular fractures, such as some sandstone rocks, for which it has been found to be close to 0.5 [10]. The same exponent  $H$  describes the scaling behavior of the two-point height correlation function, and therefore, one expects the fractal geometry of the surfaces to induce spatially correlated velocity fluctuations.

A particularly sensitive measurement of the correlated character of the velocity fluctuations is the shape of an advected front of tracer particles, because each particle position is an integral over the velocity field along its path. Recent displacement experiments have found a striking approximate correlation between tracer motion and surface geometry { the shape of the front was found to be self-affine, with an exponent close to the Hurst exponent  $H = 0.8$  of the fracture wall [12]. The objective of this paper is to establish this connection

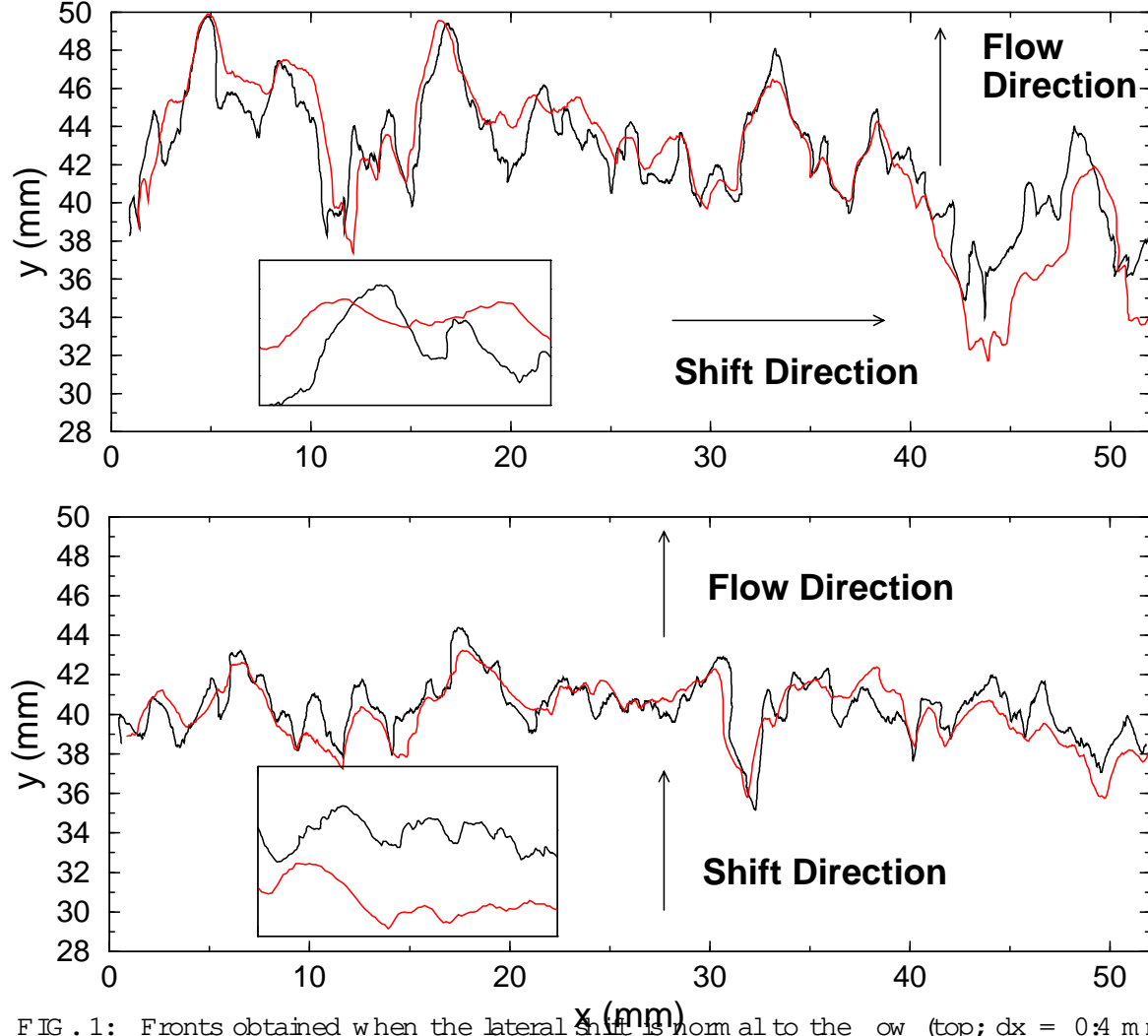


FIG. 1: Fronts obtained when the lateral shift is normal to the flow (top;  $dx = 0.4$  mm) and parallel to the flow (bottom;  $dy = 0.4$  mm). The black lines correspond to a fracture with Hurst exponent  $= 0.5$  and the gray lines correspond to  $= 0.8$ . The inserts display 4 mm  $\times$  4 mm sections of the fronts.

in quantitative detail, and determine its range of validity and further implications, using Lattice-Boltzmann (LB) numerical simulations [13]. We consider the motion of passive tracers in single fractures, which are modeled as the opening between two perfectly matching self-affine rough surfaces. We assume that there is no contact between the two fracture surfaces, and that the walls are chemically inert, completely rigid, and non-porous. As in the experiments motivating this work, we focus on the case of small Reynolds numbers for which inertia effects can be neglected, and Peclet number sufficiently high to ignore molecular diffusion.

A self-affine surface is first generated numerically, using a Fourier synthesis method [16],

and the fracture pore space is the region between one such surface and a suitably shifted replica. First, the two surfaces are separated by a fixed distance  $h$ , in the direction normal to the mean plane of the fracture, and then a lateral shift of the upper surface is introduced. The effects of the latter lateral shift, meant to reflect subsurface motion during or subsequent to fracture, are an important practical issue. The maximum allowed shift corresponds to the occurrence of the first contact point between the two surfaces, so that the fracture is open over its full area. Two orthogonal shift directions along the mean plane of the fracture are considered;  $dy$ , in the direction of the mean flow, and  $dx$ , perpendicular to it. The free space between the two surfaces is occupied by a cubic lattice of fixed lattice spacing, with  $1024 \times 1024 \times 20$  sites, which is large enough to accurately capture the three-dimensionality of the velocity field [16].

In order to generate numerically fractures that are comparable to those used in the experiments, we need to match the two relevant length scales, the topothesy and the mean aperture, as well as the Hurst exponent. Thus, the mean aperture is set to  $1 \text{ mm}$ , corresponding to a fracture size  $L = 51.2 \text{ mm}$  ( $\lambda = 0.05 \text{ mm}$ ), equal to one fourth of the fracture used in [12]. In order to have the same surface roughness, the amplitude of average fluctuations in surface height over a length of  $1 \text{ mm}$  is set to  $0.25 \text{ mm}$ . Two different values of the Hurst exponent are used here:  $0.8$  and  $0.5$ . The first value corresponds to the measured Hurst exponent of the material used in [12], and the second one is typical of fractured materials with intergranular effects. Considerable height variations occur over a distance comparable to the aperture,  $z(h) = 0.25 \text{ mm}$  and, therefore, the lubrication approximation, which assumes a Poiseuille velocity profile across the aperture, fails to describe the flow field inside the fractures [11]. Therefore, the three-dimensional flow field in the pore space of the fractures is calculated, for different values of the lateral shift, using a LB method [17]. Periodic boundary conditions are used in the  $x$  and  $y$  directions, including the inflow and outflow, and the Reynolds number is small ( $< 0.2$ ).

In the displacement experiments presented in Ref. [12], a steady radial flow of a clear fluid is first established in a transparent fracture model, cast in epoxy from natural granite. The same fluid, with a small concentration of a dye, is then injected and the spreading front of the dye is recorded. Several mechanisms contribute to the dispersion of tracer particles, among them molecular diffusion and Taylor dispersion. However, the most relevant process that drives the spreading within fractures is the velocity fluctuations induced by the sur-

$\epsilon = 0.5$	$dy = 0.4$	$dx = 0.4$	$\epsilon = 0.8$	$dy = 0.4$	$dx = 0.4$
hyi	40:40	42:56	hyi	40:1	42:4
	1:43	3:11		1:55	4:25
e	9:23	15:32	e	7:49	18:20

TABLE I: Statistical properties of the front in mm displayed in Fig. 1; hyi is the mean position of the tracers in the flow direction,  $\epsilon = h(y - hyi)^2 i^{1/2}$ , and  $e = y_{max} - y_{min}$ .

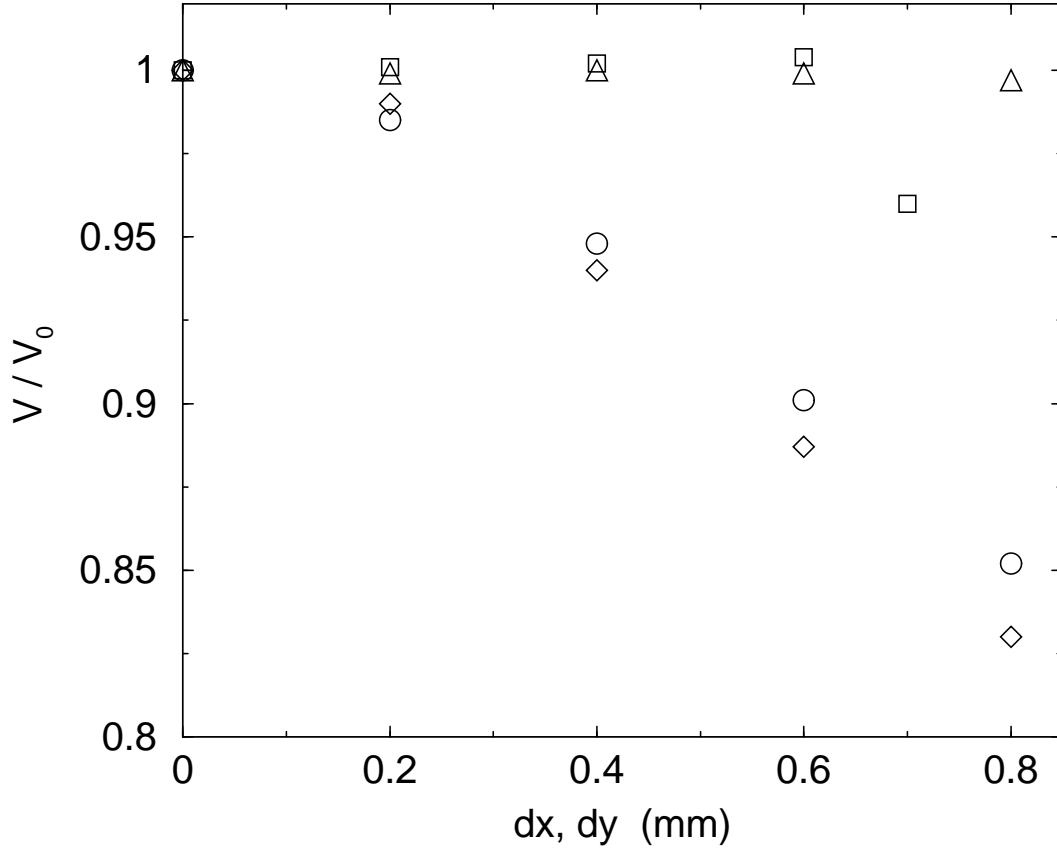


FIG. 2: Mean velocity of the tracers normalized by the velocity for zero shift as function of the shift.  $\epsilon = 0.5$  and  $\epsilon = 0.8$  are for flow along the shift direction within fractures of wall roughness  $\epsilon = 0.5$  and  $0.8$ .  $\epsilon = 0.5$  and  $0.8$  correspond to flow normal to the shift in fractures with  $\epsilon = 0.5$  and  $0.8$ .

face roughness [12]. This mechanism, known as geometric or macro-dispersion, is linear in the velocity, and therefore leads to an external front that is independent of the flow rate for a fixed injected volume. The front is thus essentially determined by the two-dimensional geometrical disorder of the velocity field in the mean fracture plane. Comparisons between experimental and numerical dispersion results can thus be achieved by considering

the spreading of tracer particles moving in the flow field resulting from averaging the three dimensional velocities over the gap of the fracture.

Initially in the computations, a tracer particle is located at each of the 1024 lattice sites corresponding to the injection side of the fracture. Each particle then propagates in the gap averaged velocity field and the velocity fluctuations due to the effective aperture variation will distort the initially flat front. Figure 1 shows typical invasion fronts obtained after the tracer traverses roughly 80% of the system. An obvious qualitative feature is that the front is rougher when the relative shift of the fracture surfaces is normal to the mean flow. Quantitatively, these small-scale features vary significantly with both the Hurst exponent and the shift direction, and in particular, the front contains more small scale details when the fracture wall roughness is decreased. The basic numerical properties of these fronts are entirely consistent with their visual appearance, as shown in Table I. We will show presently that these fronts are in fact fractals, over a range of length scales. In addition, in Fig. 2, we show that there is a remarkable anisotropy in the average propagation velocity of the front, in that a relative shift perpendicular to the mean flow has a negligible effect, whereas a shift along the flow produces a systematic decrease in the permeability. Qualitatively, this behavior may be understood from the observation that transverse shifts simply replace one preferred flow channel with another of comparable hydraulic resistance while longitudinal shifts tend to block the flow, but the systematic variation, or lack of it, seen here is quite surprising [16].

The experimental results presented in [12] were analyzed for their fractal dimension  $D$  using the average mass method [3], in which a constant density of tracer is assumed for the invasion front and the average number of tracer particles,  $\overline{M}(r)$ , located at a distance less than  $r$  from a random origin on the contour is computed. For a fractal front, a power law relationship  $\overline{M}(r) \propto r^D$  is expected, where  $D$  is the fractal dimension ranging between 1 and 2, and if the front is furthermore assumed to be self-similar, one would identify  $\zeta_f = 2 - D$ . The result found there was  $\zeta_f = 0.74 \pm 0.03$ , close to the Hurst exponent of the fractures,  $\zeta_f = 0.8$ . If we apply the same analysis to the numerical results here, we obtain [13]  $\zeta_f = 0.82 \pm 0.01$  when  $\alpha = 0.8$  and  $\zeta_f = 0.5 \pm 0.15$  for  $\alpha = 0.5$ , for length scales between certain upper and lower cutoffs. The lower cutoff is of the order the mean aperture, and independent of the direction and magnitude of the lateral shift, as were the dimensions  $\zeta_f$  themselves. However, the upper cutoff is shift-dependent, and difficult to interpret. An additional and

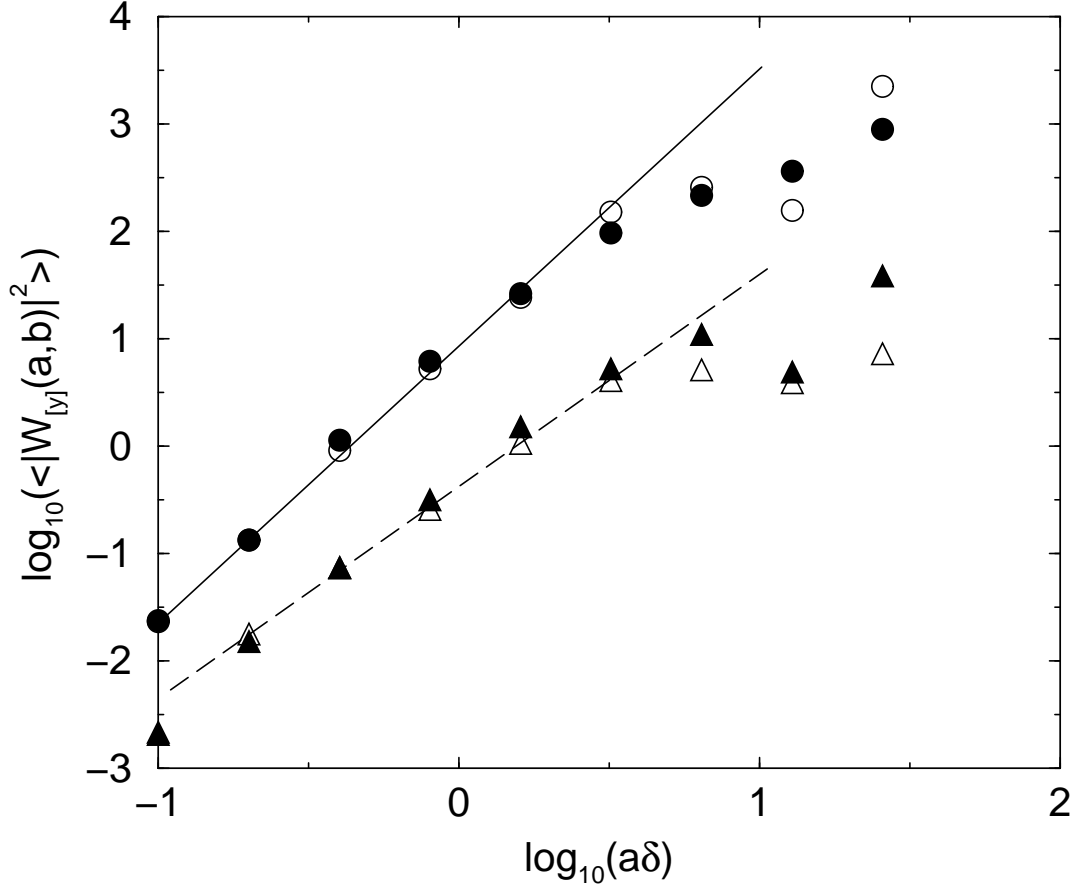


FIG. 3: Variation of  $\log_{10}(\langle |W_y(a;b)|^2 \rangle)$  as function of  $\log_{10}(a\delta)$ . Circles and triangles correspond to  $\delta = 0.8$  and  $\delta = 0.5$  respectively. Solid and open symbols correspond to  $dy = 0.4$  and  $dx = 0.4$  respectively. The two data sets are shifted vertically for convenience. The solid line has a slope of 2.6 while the dashed line has a slope of 2.

severe shortcoming of this procedure is that it does not directly test self-affinity.

A more appropriate method for self-affine structures is the average wavelet coefficient (AWC) analysis [18], where a one dimensional front  $y(x)$  is transformed into the wavelet domain as

$$W_y(a;b) = \frac{1}{\sqrt{a}} \int_a^Z \psi_{a;b}(x) y(x) dx; \quad (1)$$

where  $\psi_{a;b}(x)$  is obtained from the analyzing wavelet  $\psi$ , in our case a Daubechies wavelet [19], via rescaling and translation,  $\psi_{a;b}(x) = \psi((x-b)/a)$ . The AWC measures the average "energy" present in the front at a given scale, defined as the arithmetic average of  $|W_y(a;b)|^2$  over all possible locations  $b$ , and for a statistically self-affine profile with exponent  $\alpha_f$ , it scales

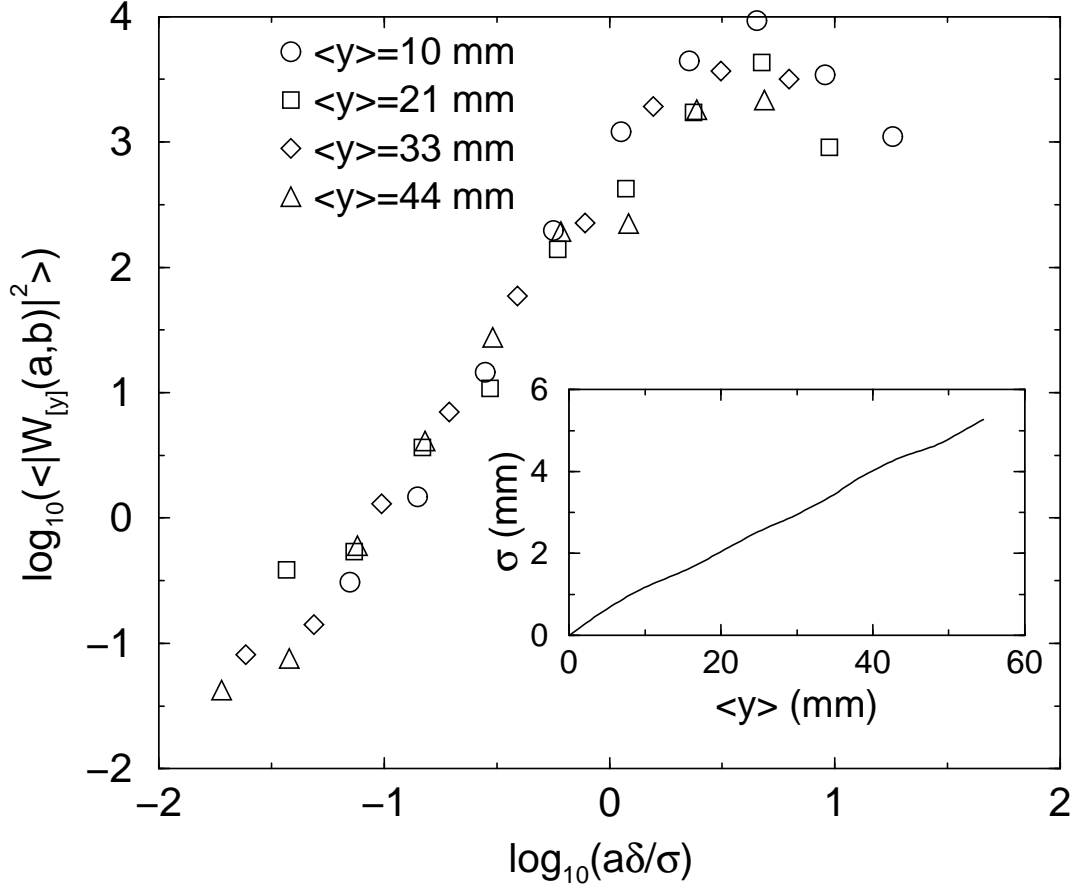


FIG. 4:  $\log_{10}(\langle |W_{[y]}(a;b)|^2 \rangle)$  as function of the normalized scale parameter  $\log_{10}(a\delta/\sigma)$ . The data set are shifted vertically to make comparisons easier. They correspond to fronts obtained after different mean traveled distances  $\langle y \rangle$ , in a fracture of roughness  $\beta = 0.3$  and with walls shifted by  $dx = 0.4$  mm. The insert shows the variation of  $\sigma$  as a function of the mean traveled distance.

as  $\langle |W_{[y]}(a;b)|^2 \rangle \propto a^{2f+1}$ . Typical results of applying the AWC method to the numerical fronts shown in Fig. 1 are given in Fig. 3, and we see a robust scaling behavior, depending only on the roughness exponent of the fracture surfaces and independent of the relative shift and the invasion time. We find  $f = 0.82 \pm 0.1$  for surfaces with roughness  $\beta = 0.3$  and  $f = 0.5 \pm 0.15$  for surfaces with  $\beta = 0.5$ , consistent with the values found using the average-mass method. These results are in good agreement with previous experimental studies of tracer dispersion [12] and with a theoretical analysis based on a perturbative approach [20].

As usual, one sees scaling behavior only between certain cutoff length scales. The origin of the upper cutoff can be understood by considering the "energy" as a function of  $a = \delta$ , where  $\delta$  is the width of the front. In Fig. 4, data for the case  $\beta = 0.3$  and  $dx = 0.4$  are



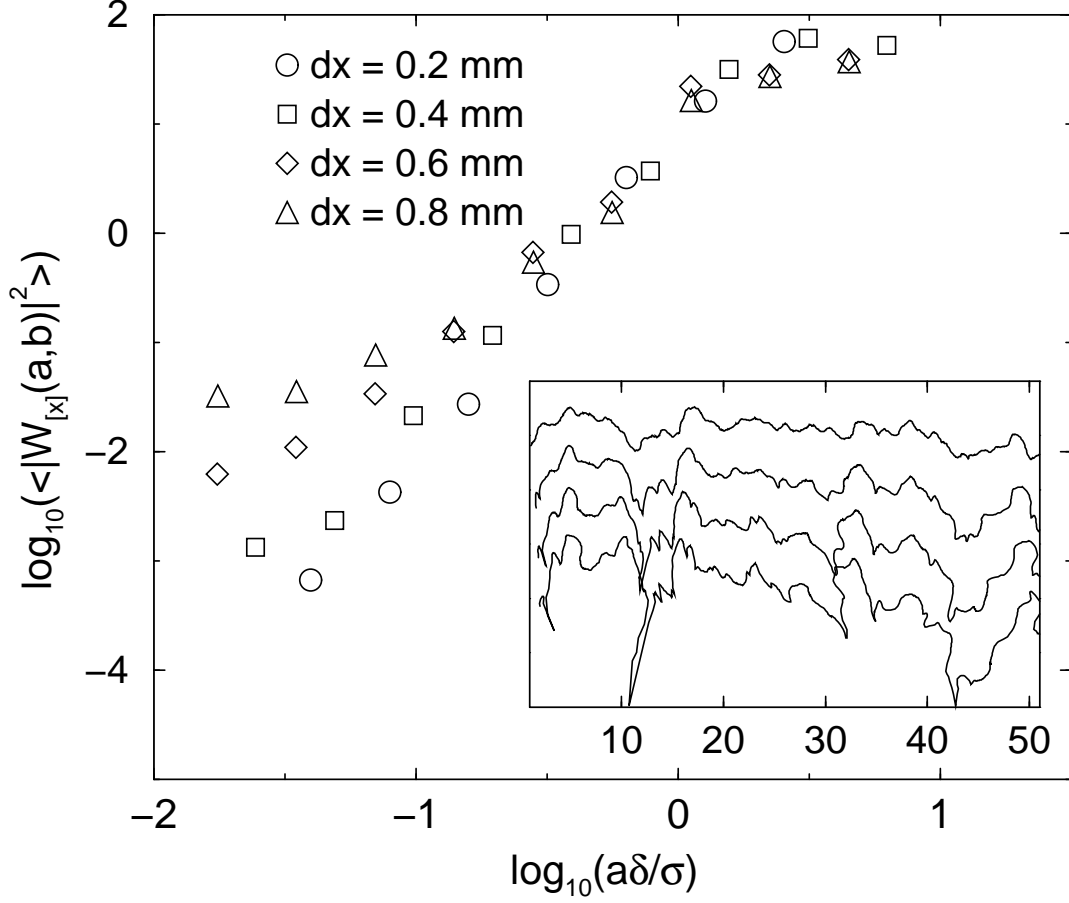


FIG. 5: Variation of  $\log_{10} \langle |W_{[x]}(a,b)|^2 \rangle$  as function of  $\log_{10}(a\delta/\sigma)$ . The data sets are shifted vertically to make comparisons easier. They correspond to fronts obtained for the same average traveled distance  $\langle y_i \rangle = 40.7$  mm and for the same fracture ( $\beta = 0.8$ ), but for different values of the lateral shift. The insert displays the corresponding fronts for increasing shifts from top to bottom.

plotted at different times, showing that the upper cutoff for scaling behavior is proportional to the width of the front. The width itself grows roughly linearly as a function of time, or equivalently with the mean distance traversed by the front, as seen in the inset of Fig. 4, so the upper limit of self-affine behavior increases with time. To understand the lower cutoff, it is instructive to compare fronts at the same mean traversed distance for different values of the shift. In Fig. 5 we display data for the  $\beta = 0.8$  fracture with different values of lateral shift, at the same transit time; the lower cutoff is seen to increase with increasing shift. The connection between scaling breakdown and shift can be elucidated by simply examining the front shapes in these four cases, as shown in the inset to Fig. 5. An increasing shift tends

to produce stagnant low-velocity regions where the front halts, and these regions destroy the self-similarity. The AWC method is particularly well-suited to address the lower cutoff issue, because the stagnant tails of the front contribute to the wavelet "energy" strongly at low values of  $a$ . In the average-mass method, in contrast, they contribute predominantly at large  $r$  whereas the lower cutoff is on the order of the mean aperture, independent of the surface exponent and any lateral shift [12, 13].

There is an obvious intuitive appeal to the idea that a fractal geometry will somehow impose itself on a suitably flexible object propagating through it. In this paper we have used numerical simulations to expand upon the experimental observation that a (high Peclet number) displacement front in a self-affine fracture behaves in this way. We have presented compelling evidence that self-affine fronts indeed appear in this situation, for a wide range of parameters, and have further determined the relevant range of length scales for scaling behavior. This work raises a number of further intriguing questions, including (1) The behavior of higher moments of the front geometry; (2) The interplay between the self-affine character and the strong anisotropic behavior in radial injection flows; (3) The effects of finite Peclet numbers, which would presumably alter the scaling cutoff lengths, on hydrodynamic dispersion. We hope to address these and other questions in future work.

We have benefited from discussions with S. Roux. HA and JPH are supported by the CNRS and ANDRA through the GdR FORPRO (contribution No. 2003=12A). This work was partly supported by the ECODEV and PNRH CNRS programs. GD and JK are supported by the Geosciences Program of the Office of Basic Energy Sciences, US Department of Energy. Computer resources were provided by the National Energy Research Scientific Computing Center. This work was facilitated by a CNRS-NSF Collaborative Research Grant.

- 
- [1] C.A. Morrow and L.Q. Shi, J. Phys. A 84, 3193 (1984).
  - [2] E. Hakami and E. Larsson, Int. J. Rock Mech. Min. Sci. & Geomech. Abstr. 33, 395 (1996).
  - [3] J. Feder, Fractals (Plenum, New York, 1988).
  - [4] B. Mandelbrot, The Fractal Geometry of Nature (W.H. Freeman, New York, 1982).
  - [5] B.B. Mandelbrot and D.E. Passoja and A.J. Paulay, Nature 308, 721 (1984).

- [6] E. Bouchaud, G. Lapasset, and J. P. Lesieur, Europhys. Lett. 13, 73 (1990).
- [7] J. Kertész, V. K. Horváth and F. Weber, Fractals 1, 67 (1996).
- [8] S. Brown and C. Scholz, J. Geophys. Res. 90, 12575 (1985).
- [9] C. Poon, R. Sayles, and T. Jones, J. Phys. D : Appl. Phys. 25, 1269 (1992).
- [10] J. M. Bona, C. Allain and J. P. Hulin, European Phys. J. - App. Phys. 2, 2 (1998).
- [11] V. V. Mourzenko, J.-F. Thovert and P. M. Adler, J. Phys. II France 5, 465 (1995).
- [12] H. Auradou, J. P. Hulin and S. Roux, Phys. Rev. E 63, 066306 (2001).
- [13] We have used particular examples taken from extensive numerical simulations to draw our conclusions; further details and analysis will be provided in a longer paper now in preparation.
- [14] G. Drazner and J. Koplik, Phys. Rev. E 62, 8076 (2000).
- [15] G. Drazner and J. Koplik, Phys. Rev. E 63, 056104 (2001).
- [16] G. Drazner and J. Koplik, Phys. Rev. E 66, 026303 (2002).
- [17] Y. H. Qian and D. d'Humières and P. Lallemand, Europhys. Lett. 17, 479 (1992).
- [18] I. Simonsen, A. Hansen and O. M. N. Nes, Phys. Rev. E 58, 2779 (1998).
- [19] I. Daubechies, Ten Lectures on Wavelets (SIAM, Philadelphia, 1992).
- [20] S. Roux, F. Bouraboué and J. P. Hulin, Transp. Porous Media 32, 97 (1998).